Automatic Segmentation of Left Atrial Scar from Delayed-Enhancement Magnetic Resonance Imaging

Rashed Karim[1], Aruna Arujuna[1,2], Alex Brazier[1], Jaswinder Gill[1,2], C. Aldo Rinaldi[1,2], Mark O'Neill[1,2], Reza Razavi[1,2], Tobias Schaeffter[1], Daniel Rueckert[3], and Kawal S. Rhode[1]

[1] Division of Imaging Sciences and Biomedical Engineering, King's College London, UK
[2] Department of Cardiology, Guy's and St. Thomas' Hospitals NHS Trust, London, UK
[3] Department of Computing, Imperial College London, London, UK
{rashed.karim,aruna.arujuna,alex.brazier,
tobias.schaeffter,kawal.rhode}@kcl.ac.uk,
{jaswinder.gill,aldo.rinaldi,mark.oneill}@gstt.nhs.uk,
d.rueckert@imperial.ac.uk

Abstract. Delayed-enhancement magnetic resonance imaging is an effective technique for imaging left atrial (LA) scars both pre- and post- radio-frequency ablation for the treatment of atrial fibrillation. Existing techniques for LA scar segmentation require expert manual interaction making them tedious and prone to high observer variability. In this paper, we propose a novel automatic segmentation algorithm for segmenting LA scar based on a probabilistic tissue intensity model. This is implemented as a Markov random field-based energy formulation and solved using graph-cuts. It was evaluated against an existing semi-automatic approach and expert manual segmentations using 9 patient data sets. Surface representations were used to compare the methods. The segmented LA scar was expressed as a percentage of the total LA surface. Statistical analysis showed that the novel algorithm was not significantly different to the manual method and that it compared more favorably with this than the semi-automatic approach.

Keywords: delayed enhancement MRI, atrial fibrillation, scar segmentation, graph-cuts, Markov random fields.

1 Introduction

Atrial fibrillation (AF) is the most common cardiac arrhythmia and affects approximately 2.2 million people in the USA. A common treatment for AF is minimally-invasive catheter-based radio-frequency ablation (RFA) that aims to electrically isolate the pulmonary veins (PVs) from the left atrial body. The procedure is successful in 50-80% of patients. Assessment of the LA substrate in terms of scarring is important both pre- and post-RFA. The successful imaging of LA scars has been demonstrated using Gadolinium delayed enhancement (DE) magnetic resonance imaging (MRI) [1, 2] (see Fig. 1a). However, clinical interpretation of these data is difficult from tomographic images. Several strategies have been proposed for visualization including maximum intensity projection (MIP) onto a thick slice [1],

D.N. Metaxas and L. Axel (Eds.): FIMH 2011, LNCS 6666, pp. 63–70, 2011.

MIP onto a LA surface model [3] (see Fig. 1b), and 3D volume rendering [2]. Such visualization techniques provide more intuitive visualization and may have a role for guiding redo procedures [4], which are very common (20-50%). Quantification of the DE-MRI has been proposed using thresholding techniques for either endocardial surface-based segmentation [3] or volumetric segmentation [2]. Such quantification has been shown to predict likely response to RFA in clinical studies [5]. It will also be critical for applying cardiac biophysical models of AF for patient selection and RFA planning [6].

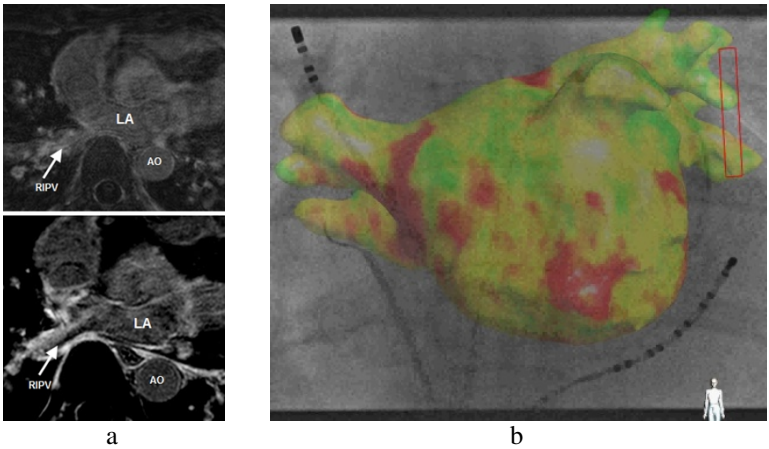

Fig. 1. (a) Example of left atrial Gadolinium delayed enhancement MR images; (top) pre-ablation; (bottom) post-ablation showing enhancement around the pulmonary veins. (b) Left atrial surface model with color-code scar information (red is scar) generated using maximum intensity projection of DE-MRI intensity to left atrial surface along surface normals [3]. The model is superimposed onto live X-ray fluoroscopy data to guide a redo ablation procedure.

Existing techniques [2, 3] for LA scar segmentation require expert user interaction making them tedious and prone to high inter- and intra-observer variability. In this paper, we propose a novel automatic LA scar segmentation algorithm based on a probabilistic tissue intensity model of DE-MRI data. This is implemented as a Markov random field (MRF)-based energy formulation and solved using graph-cuts. We evaluated our automatic method using 9 patient data and compare to expert manual and semi-automatic approaches [3].

2 Methods

2.1 Patient Protocol

9 patients with paroxysmal AF were recruited into the study under a local ethics committee approved protocol. The patients underwent RFA using wide area circumferential ablation to achieve isolation of the PVs. At 6 months post-ablation, the patients underwent MRI (1.5T Achieva, Philips Healthcare, The Netherlands).

The MR examination included (a) a 3D magnetic resonance angiography (MRA) scan with whole-heart coverage, reconstructed to 1mm isotropic resolution, following injection of a 0.4ml/kg double dose of a Gd-DTPA contrast agent; (b) a 3D respiratory-navigated and cardiac-gated, balanced steady state free precession (bSSFP) acquisition with whole-heart coverage, reconstructed to 1.3mm isotropic resolution; and (c) 20 minutes after contrast injection, the delayed enhancement scan, which was a 3D respiratory-navigated and cardiac-gated, inversion recovery turbo field echo with whole LA coverage, reconstructed to 1.3x1.3x2mm^3 resolution.

2.2 Left Atrium Segmentation and Image Registration

The best quality anatomical scan was selected from either the bSSFP or MRA scans and the endocardial boundary of the LA was segmented using an automatic approach based on a statistical shape model [7]. The automatic segmentation was verified by a clinical expert and manual corrections were made whenever required to achieve a high-fidelity result. The anatomical images were registered to the DE images using initialization by the DICOM header data, followed by affine registration [8]. Thereby the endocardial LA boundary was defined in the DE images.

2.3 Segmentation of Atrial Lesions

Segmentation Framework. The segmentation approach is based on a MRF-based energy formulation solved using graph-cuts [9]. Segmentation of scars from DE-MRI images can be described as assigning a label $f_p \in \{0,1\}$ to every voxel p in the image. Voxels representing scar tissue are assigned to the foreground class label $f_p = 1$ and non-scar tissues are assigned to the background class label $f_p = 0$. Given the observed intensities in the image and prior knowledge about scars, the segmentation problem can be solved using a probabilistic framework where the maximum *a posteriori* (MAP) estimate is computed using Bayes' theorem:

$$\text{argmax}_{\mathbf{f}}\, p(\mathbf{f}|\mathbf{I}) = \frac{p(\mathbf{I}|\mathbf{f})p(\mathbf{f})}{p(\mathbf{I})} \tag{1}$$

where $\mathbf{f}$ is the total label configuration and $\mathbf{I}$ are all observed intensities in the image. The image likelihood $p(\mathbf{I}|\mathbf{f})$ describes how likely is the observed image given a label configuration $\mathbf{f}$. The prior $p(\mathbf{f})$ encodes any prior knowledge of the tissue class labels (i.e. non-scar and scar tissue classes). Eq. 1 is commonly transformed into an MRF-based energy function over the neighborhood system N and labeling f:

$$E(f) = \lambda \sum_{p \in P} E_{\text{data}}(f_p) - \sum_{\{p,q\} \in N} E_{\text{prior}}(f_p, f_q). \tag{2}$$

The introduction of a weighting term λ weights the influence of the energy terms. The intensity energy E_{data} measures the disagreement between the *a prior* probabilistic model and the observed data, and E_{prior} is a smoothness term within a tissue class that penalizes any discontinuities between voxel pairs $\{p, q\}$. The scar segmentation problem is solved by minimization of the energy function described in Eq. 2. In the context of images, certain MRF-based energy functions are efficiently solved using

graph-cuts [9]. In this approach the image is represented as a graph $G = \langle V, E \rangle$ where each voxel in the image corresponds to a node. However, the node set V contains two special *terminal* nodes called the *source* and the *sink.* These represent the foreground (i.e. scar) and background (i.e. non-scar tissue) classes respectively. Every node in the graph has an edge to these terminal nodes, as well as neighbour-to-neighbour edge links that exist between neighboring nodes. The MRF-based energy function in Eq. 2 is coded into the edge weights. The optimal *cut* or partitioning of the graph into two disjoint sets with each set containing a terminal node solves the segmentation problem. The cost of the graph-cut is equal to the total energy of the corresponding segmentation.

Non-scar Tissue Priors. The intensity model for non-scar tissue provides the source edge weights in the graph. This is based on prior knowledge about different tissue classes that could possibly interface with scar. As scar tissue normally borders with a multitude of tissues, it is not possible to model non-scar tissues using a single, uni-modal Gaussian distribution. A multi-modal distribution is used that can be represented as a mixture of Gaussian distributions:

$$\sum_{i=1}^{n} a_i \, \mathbf{G}_i(\mu_i, \sigma_i) \tag{3}$$

where $\mathbf{G}_i$ is a Gaussian distribution for tissue i with mean μ_i and variance σ_i for some mixture proportion $a_i \in [0,1]$ and $\sum_{i=1}^{n} a_i = 1$. The non-scar tissue model is derived from the image to be segmented (i.e. unseen image). Given our segmentation of the LA endocardium from the anatomical images, regions of blood pool, atrial wall and pericardium can be approximated. This is accomplished by obtaining regions within fixed distances from the LA endocardium. For example, regions of blood pool and pericardium are obtained 5mm inside and outside the endocardial border, respectively. The atrial wall region is obtained 0-5 mm from the endocardium. See Fig. 2 for examples of the healthy tissue mixture model taken from two patients. However, as scarred tissue is also part of the atrial wall, the Gaussian in the mixture model most likely resulting from scar tissue is identified and eliminated. This is possible using an ROI corresponding to scar tissue that is selected by the operator. Assuming that the mean and variance of scar are μ_S and σ_S^2 respectively, then the Gaussian corresponding to index t has the maximum amount of overlap with the scar Gaussian within unit standard deviation and is subsequently eliminated:

$$t = \text{argmax}_i \big| |\mu_i \pm \sigma_i| - |\mu_S \pm \sigma_S| \big|. \tag{4}$$

Following the elimination of Gaussian $\mathbf{G}_t$, the weights of the remaining Gaussians of the mixture model are normalized to sum to one. It is also useful to take as user-input an ROI on normal myocardium selected by the operator. To incorporate this new normal myocardium Gaussian with mean and variance μ_M and σ_M into the existing tissue mixture model, the weights are adjusted based on ρ which weights the degree of confidence on the manual operator's normal myocardium selection with a higher ratio assigned for expert operators:

$$p\big(\mathbf{I} \big| f_p = 0\big) = (1-\rho) \sum_{i=1}^{n-\{t\}} a_i \, \mathbf{G}_i(\mu_i, \sigma_i) + \rho \mathbf{G}(\mu_M, \sigma_M). \tag{5}$$

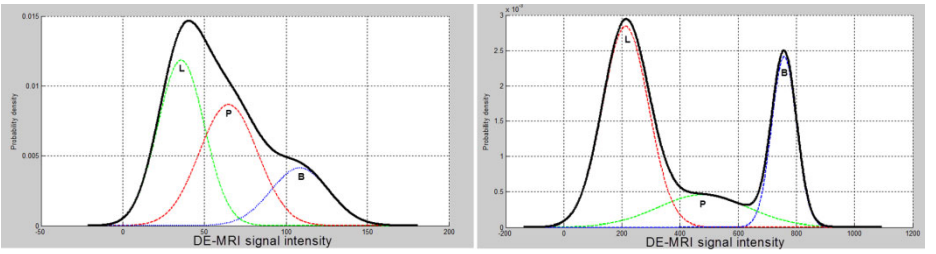

Fig. 2. The healthy tissue model computed in two patients. A Gaussian mixture density curve (in bold) is computed from individual Gaussians of the three tissue classes (L – lungs, P – pericardium, B – blood pool).

The parameters (a_i, μ_i, σ_i) of the Gaussian mixture model are obtained using the Expectation-Maximization (EM)-algorithm [10].

Scar Tissue Priors. The intensity model for scar is built from training data. This model corresponds to the intensity energy E_{data} in the MRF model (Eq. 2), and thus the sink edge weights in the flow-graph G. Scar tissue appears predominantly as areas of bright regions in DE-MRI. To derive an intensity distribution model for scar tissues, a Gaussian density function can be used:

$$p(\mathbf{I}|f_p = 1) = \frac{1}{\sqrt{2\pi\sigma^2}} \exp\left[-\frac{1}{2}\left(\frac{r-\mu}{\sigma}\right)^2\right] \tag{6}$$

where r is the ratio of DE-MRI signal of scar tissue to interfacing tissues with mean μ and variance σ. These are tissue classes which could possibly interact with scar tissues in the image. The parameters μ and σ are derived from training images which are expert hand-segmentations of scars in DE-MRI. The ratio r for each voxel in the unseen image is determined as the ratio of its intensity to mean blood pool and pericardium intensity.

Tissue Class Boundaries for Smoothness. To ensure continuity and smoothness within voxels of a tissue class through the E_{prior} term of the MRF energy function, neighboring voxels sharing similar intensities incur an exponentially high cost if they are classified into different tissue classes. The Lorentzian error norm [11] is employed, which is a robust metric for measuring intensity differences within a neighborhood:

$$\zeta(p,q) = \left(1 + \frac{1}{2}\left(\frac{|I_p - I_q|}{\sigma}\right)^2\right). \tag{7}$$

The scale σ can be estimated from the DE-MRI image and depends on the variance of the *actual* scar and non-scar tissue class intensity distributions. With decreasing scale, the algorithm becomes less forgiving to small difference in intensities. Given that it is technically challenging to acquire high quality DE-MRI scans that show a clear distinction between scar and non-scar tissue, a larger value for the scale σ is almost always preferred. For convenience, neighbour-to-neighbour edge links are

bounded above and below by $[0,1]$ and thus the edge-link weight assigned between neighbouring nodes is simply given by $1/(1+\zeta(p,q))$.

2.4 Evaluation of Novel Approach

The proposed automatic algorithm was evaluated with the 9 patient data using the leave-one-out principle, with 8/9 data used for training and 1/9 used as the unseen data. For comparison, the LA scars were manually segmented by two expert observers using the ITKSnap tool (www.itksnap.org). Furthermore, each data set was processed using the previously published semi-automatic approach of Knowles et al. [3]. This approach projects the maximum signal intensity from the DE data onto the LA endocardial surface along the surface normals. The segmentation is then achieved by applying a user-interactive threshold on the projected data. In order to make a comparison between the automatic, semi-automatic and manual segmentations, all segmentation results were projected onto the LA endocardial surfaces. All processing was carried out a 2.8 GHz PC.

3 Results

The pre-processing (LA segmentation and registration) was the same for each approach, i.e. automatic, semi-automatic and manual, and took typically 5 minutes. The novel automatic algorithm completed the segmentation process for each DE image in typically 30 seconds whereas the semi-automatic approach took typically 5 minutes. Manual segmentation of the scars took typically 45 minutes. See Fig. 3 for example results.

For each segmentation method, the amount of detected scar expressed as a percentage of the total LA surface was calculated (Fig. 4). Segmentations using the automatic algorithm approximated more closely to the manual segmentations than

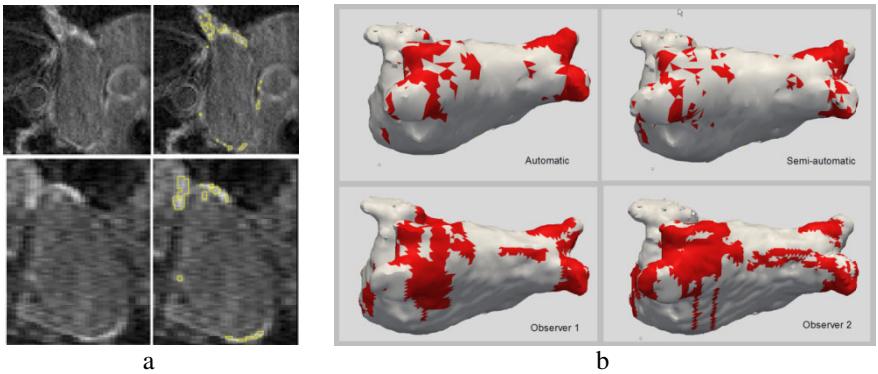

a b

Fig. 3. Results from segmentation methods. (a) Automatic segmentations for patient 1 showing 2 example slices from the DE-MRI data; (left) original image data; (right) with segmentation annotations. (b) Surface representations for segmentations results for patient 2 showing automatic, semi-automatic and manual segmentations.

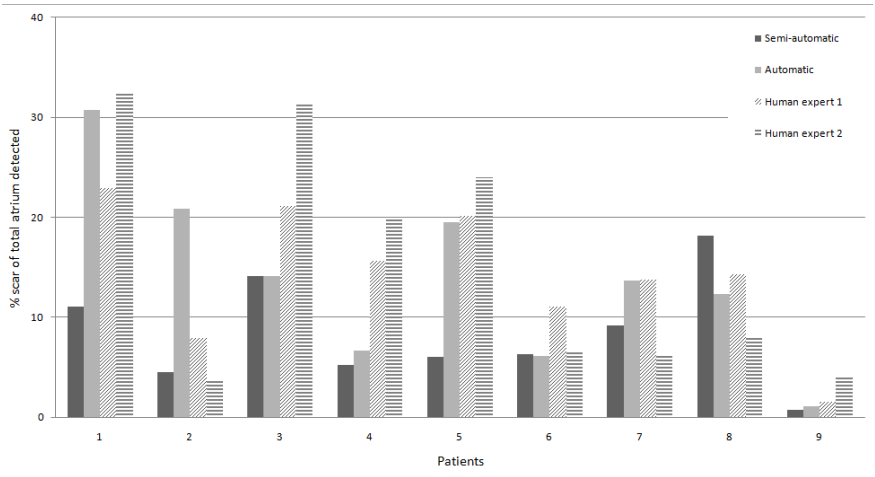

Fig. 4. Comparison of percentage scar in each patient for the different methods. Detected scar was expressed as a percentage of total LA surface.

Table 1. *p*-values from paired t-tests between each method with significant differences underlined. The significance level was set at 0.05.

p-values	Semi-auto	Auto	Observer 1	Observer 2
Semi-auto		0.09	0.10	0.01
Automatic			0.72	0.87
Observer 1				0.70

those using semi-automatic method, as confirmed this using a statistical paired *t*-test (Table 1). At a significance level of 0.05, there was no significant difference between the percentage scar detected in automatic and manual methods. In contrast, a significant difference was found between semi-automatic and one of the expert observers.

4 Discussion and Conclusion

In this paper, we have presented a novel automatic technique for segmenting scars in the LA using DE-MRI. The technique was applied to 9 patient data sets and the results compared to expert manual segmentations and segmentations from an existing semi-automatic approach. The automatic method was not significantly different from the manual method and compared more favorably to this than the semi-automatic approach. Furthermore, using the automatic method produces a considerable time-saving over using manual segmentation (30 seconds vs. 45 minutes) and some saving over the using semi-automatic method (30 seconds vs. 5 minutes). Most importantly, the automatic method results in a volumetric segmentation as opposed to a surface

segmentation, as for the semi-automatic method. This will be important for assessing transmurality of post-RFA scars. It is envisaged that user-independent lesion segmentation with low computational cost, as proposed in this paper, will allow for standardization of DE-MRI as a marker of cardiac injury. Future work will focus on improved training of the probabilistic intensity model and validation using a larger patient cohort with more expert segmentations per data set.

References

[1] Peters, D.C., Wylie, J.V., Hauser, T.H., Kissinger, K.V., Botnar, R.M., Essebag, V., Josephson, M.E., Manning, W.J.: Detection of pulmonary vein and left atrial scar after catheter ablation with three-dimensional navigator-gated delayed enhancement MR imaging: initial experience. Radiology 243(3), 690–695 (2007)

[2] McGann, C.J., Kholmovski, E.G., Oakes, R.S., Blauer, J.J., Daccarett, M., Segerson, N., Airey, K.J., Akoum, N., Fish, E., Badger, T.J., DiBella, E.V., Parker, D., MacLeod, R.S., Marrouche, N.F.: New magnetic resonance imaging-based method for defining the extent of left atrial wall injury after the ablation of atrial fibrillation. J. Am. Coll. Cardiol. 52(15), 1263–1271 (2008)

[3] Knowles, B.R., Caulfield, D., Cooklin, M., Rinaldi, C.A., Gill, J., Bostock, J., Razavi, R., Schaeffter, T., Rhode, K.S.: 3-D visualization of acute RF ablation lesions using MRI for the simultaneous determination of the patterns of necrosis and edema. IEEE Trans. Biomed. Eng. 57(6), 1467–1475 (2010)

[4] Reddy, V.Y., Schmidt, E.J., Holmvang, G., Fung, M.: Arrhythmia recurrence after atrial fibrillation ablation: Can magnetic resonance imaging identify gaps in atrial ablation lines? Journal of Cardiovascular Electrophysiology 19(4), 434–437 (2008)

[5] Oakes, R.S., Badger, T.J., Kholmovski, E.G., Akoum, N., Burgon, N.S., Fish, E.N., Blauer, J.J., Rao, S.N., DiBella, E.V., Segerson, N.M., Daccarett, M., Windfelder, J., McGann, C.J., Parker, D., MacLeod, R.S., Marrouche, N.F.: Detection and quantification of left atrial structural remodeling with delayed-enhancement magnetic resonance imaging in patients with atrial fibrillation. Circulation 119(13), 1758–1767 (2009)

[6] Reumann, M., Bohnert, J., Seemann, G., Osswald, B., Dössel, O.: Preventive ablation strategies in a biophysical model of atrial fibrillation based on realistic anatomical data. IEEE Trans. Biomed. Eng. 55(2 Pt 1), 399–406 (2008)

[7] Peters, J., Ecabert, O., Meyer, C., Schramm, H., Kneser, R., Groth, A., Weese, J.: Automatic whole heart segmentation in static magnetic resonance image volumes. Med. Image Comput. Comput. Assist. Interv. 10(Pt 2), 402–410 (2007)

[8] Schnabel, J.A., Rueckert, D., Quist, M., Blackall, J.M., Castellano-Smith, A.D., Hartkens, T., Penney, G.P., Hall, W.A., Liu, H., Truwit, C.L., Gerritsen, F.A., Hill, D.L.G., Hawkes, D.J.: A generic framework for non-rigid registration based on non-uniform multi-level free-form deformations. Med. Image Comput. Comput. Assist. Interv. 4, 573–581 (2001)

[9] Boykov, Y., Veksler, O., Zabih, R.: Fast approximate energy minimization via graph cuts. IEEE Transactions on Pattern Analysis and Machine Intelligence 23(11), 1222–1239 (2002)

[10] Dempster, A.P., Laird, N.M., Rubin, D.B.: Maximum likelihood from incomplete data via the EM algorithm. Journal of the Royal Statistical Society, Series B (Methodological) 39(1), 1–38 (1977)

[11] Rousseeuw, P.J., Leroy, A.M.: Robust regression and outlier detection. Wiley Series in Probability and Statistics. John Wiley & Sons Inc., Chichester (1987)